Princeton Plasma Physics Laboratory

PPPL- 4954

PPPL- 4954

# Three Dimensional Equilibrium Reconstruction on the DIII-D Device

S.A. Lazerson
and the DIII-D Team

November 2013

**Prepared for the U.S. Department of Energy under Contract DE-AC02-09CH11466.**

# Princeton Plasma Physics Laboratory
# Report Disclaimers

---

## Full Legal Disclaimer



## Trademark Disclaimer



---

# PPPL Report Availability

## Princeton Plasma Physics Laboratory:

http://www.pppl.gov/techreports.cfm

## Office of Scientific and Technical Information (OSTI):

http://www.osti.gov/bridge

---

**Related Links:**

**U.S. Department of Energy**

**Office of Scientific and Technical Information**

**Fusion Links**

# Three Dimensional Equilibrium Reconstruction on the DIII-D Device

‡

**S. A. Lazerson**

Princeton Plasma Physics Laboratory, Princeton, NJ

**and the DIII-D Team**

**Abstract.** The presence of toroidal variation in diagnostic measurements indicates that the two dimensional symmetry of Tokamak equilibria is violated when resonant magnetic perturbations (RMPs) are applied to suppress edge localized modes (ELMs). While Tokamak control is still possible with a 2D model, questions arise regarding the applicability of 2D equilibria when performing detailed analysis. In particular, questions regarding edge physics would benefit from equilibrium calculations which are consistent with measurements indicating toroidal variations. The ability to fit three dimensional equilibria to diagnostic measurements has long been a challenge for non-axisymmetric devices with an inherently 3D field structure. The STELLOPT code provides a solution to such a challenge by fitting 3D VMEC equilibria to magnetic, Thomson, motional Stark effect (MSE), and charge exchange diagnostics. The plasma of the DIII-D tokamak with applied $n = 3$ RMP is reconstructed with STELLOPT, where ELM were present throughout the shot. The reconstruction is constrained by magnetic diagnostics, Thomson scattering, charge-exchange spectroscopy, and MSE polarimetry. The reconstructed equilibria posses flat spots at low order rationals associated with the applied RMP spectrum, indicating mode penetration for this shot. Boundary displacements on the order of 0.5 cm peak-to-peak were present. This suggests that while the 3D effect was small relative to the plasma minor radius, resonant mode penetration occurred, indicating the ability of 3D reconstructions to resolve key small features in the plasma.

PACS numbers: 52.55.-s

*Keywords*: Fusion, Magnetics, Diagnostics, Equilibrium, Reconstruction

Submitted to: *Plasma Phys. Control. Fusion*

## 1. Introduction

The application of 3D fields [1, 2] and measurement of helical axis states in Tokamaks [3] suggests that 2D models of the plasma response are not always adequate for interpretation of experimental measurements. This is highlighted by the process known as experimental equilibrium reconstruction, where theoretical equilibrium models are fit to experimental measurements in an attempt to better understand unmeasurable or difficult to measure quantities. For decades the Tokamak community has relied upon EFIT which utilizes a 2D axisymmetric plasma model for reconstruction purposes [4]. It has been shown that this model, at times, may not be correct when multiple toroidal locations of experimental data are input [5, 6]. Furthermore, direct interpretations of the experimental data show a toroidal variation in magnetic signals [7]. The application of resonant magnetic perturbations (RMPs) to suppress edge localized modes (ELMs) highlights the need to fit 3D equilibria to diagnostic measures. Here 3D fields are applied, breaking the axisymmetry of the device. Accurate and detailed modeling of the 3D equilibrium physics is key to interpreting the role these non-axisymmetric field play in suppressing ELMs. Furthermore, correction of error fields in Tokamaks centers around compensating the resonant fields as opposed canceling the total error fields. It is then possible that the non-resonant field may still deform the plasma, breaking axisymmetry. There is a clear need for 3D reconstruction tools among the Tokamak community.

For decades the stellarator community has been conducting experimental reconstruction with 3D magnetic geometries [8, 9]. The static nature of low-beta stellarators initially motivated reconstructions based upon look-up tables of pre-calculated equilibria [10, 11, 12]. As higher beta was achieved and more detailed diagnostics were added to stellarator experiments, experimental reconstruction required a more sophisticated approach. To this end the V3FIT [9] code was developed, and the STELLOPT code [13], originally developed for experimental design, was modified. These codes fit 3D equilibrium models of the plasma to diagnostic measurements in experiments. In this paper, a three dimensional equilibrium reconstruction of the DIII-D tokamak plasma using the STELLOPT code is presented. This device was chosen as it is highly diagnosed and has extensively documented the use of RMPs to suppress ELMs. Section 2 outlines the code, equilibrium model, and synthetic diagnostics utilized for reconstruction. Section 3 presents shot 142603 and the reconstructed 3D equilibrium by STELLOPT. Section 4 discusses the results and future work.

## 2. Method

The STELLOPT code was developed to fit the VMEC 3D ideal MHD equilibrium model [14] to target parameters using either a modified Levenberg-Marquardt, genetic, or differential evolution algorithm [15, 16]. Experimental reconstruction is made possible through the implementation of experimental diagnostic measurements as target functionals in the optimization routines. The target parameters for reconstruction of DIII-D shot 142603 have been the full set of magnetic probes, flux loops, measured plasma current, Thomson scattering electron density and temperature measurements, charge-exchange recombination ion temperature measurements, motional stark effect polarimetry measurements, and interferometric measurements of the line integrated electron density. The VMEC MHD equilibrium is

fit to these measurements through variation of the equilibrium total enclosed toroidal flux, net toroidal current, electon density profile, electron temperature profile, ion temperature profile, pressure scaling factor, vacuum field coil currents, and plasma current profile. These measurements provide 311 constraints to which 63 independent parameters are fit using the Levenberg-Marquardt algorithm.

### *2.1. Modified Levenberg-Marquardt Algorithm*

The goal of experimental reconstruction is to fit an equilibrium model to a set of target parameters $y_i$ in a least squared sense. Here the equilibrium is defined by a set of input parameters $x_j$. One seeks a set of optimization parameters $x_j$ such that

$$F\left(x_1 ... x_j\right) = \sum_{i=1}^{m} \left[ \frac{y_i - f_i\left(x_1 ... x_j\right)}{\sigma_i} \right]^2 \tag{1}$$

is a minimum, where $m$ is the number of target data points, $f_i$ are associated evaluations of the fit function, and $\sigma_i$ are associated weighting values for each target data point. For reconstruction the values of $\sigma$ are based on a tradeoff between experimental error bars associated with each measure and equal preferential weighting toward more unique measures (e.g. smaller $\sigma$ for Thomson than magnetics). The iterative scheme assumes a solution of the form

$$f\left(x_j + \delta\right) \sim f\left(x_j\right) + J\delta \tag{2}$$

where $J$ is the gradient of the function $f$ with respect to $x_j$. Optimization is the process by which $\delta$ is determined. While many methods exist for achieving such a goal, a modified Levenberg-Marquardt algorithm has been employed here. The Levenberg-Marquardt algorithm as found in the NETLIB libraries (LMDIF) has been modified for execution on parallel computers. Each processor evaluates the match to targets for a given forward difference of an input parameter. As a result, the evaluation time for the Jacobian scales as the number of varied input parameters divided by the number of available processors. In principle, it is possible that this step can take less time than a full equilibrium evaluation, assuming enough processors and the ability to start from a previously evaluated equilibria. The evaluation direction is reversed in future evaluations if, for a given variable, the function shows an increase in $F$. This is done in an attempt to force the forward difference to always search along directions of decreasing $F$.

At the minimum of our functional, the gradient of $F$ with respect to $\delta$ will be zero. To first order the minimum in $F$ can be written

$$\mathbf{F_{min}}\left(x_j + \delta\right) \sim ||\mathbf{y} - \mathbf{f}\left(x_j\right) - \mathbf{J}\delta||^2 \tag{3}$$

where we've switched to vector notation and $J$ is the Jacobian matrix. Taking this equation to be zero and including a dampening factor $\lambda$ we obtain the Levenberg-Marquardt equation for $\delta$

$$\left[\mathbf{J^T J} + \lambda\, diag\left(\mathbf{J^T J}\right)\right] \delta = \mathbf{J^T}\left[\mathbf{y} - \mathbf{f}\left(x_j\right)\right]. \tag{4}$$

The proper choice of $\lambda$ may vary depending on the problem begin examined. Here the parallelization of the code allows a search to be performed. Each processor calculates the function for a different value of $\lambda$ allowing a search to be performed along the 'Levenberg trajectory'. For small values of $\lambda$ the algorithm mimics a Gauss-Newton algorithm. For large values of $\lambda$ the algorithm mimics the gradient descent algorithm.

It is possible that during the forward differencing step lower values of $F$ will be found than those obtained by a step along the Levenberg trajectory. This is attributed to a high non-linearity between input parameters. To address this possibility, an orthogonal search is performed in parameter space. This often allows the optimizer to access new minima it may have otherwise missed.

Once the algorithm has determined the optimal fit of the input parameters to the experimental measurements, metrics for those parameters may be computed. The asymptotic standard parameter errors provide a measure of the effect of variability in the dataset to variability in the solution and is given by

$$\sigma_\beta = \sqrt{diag\left(\left(\mathbf{J^T W J}\right)^{-1}\right)}. \tag{5}$$

This provides a measure of how well constrained the model is by the given set of experimental measures. Here $W$ are the weight values calculated from

$$w_i^2 = \frac{\left(y_i - f_i\left(x_j\right)\right)^T \left(y_i - f_i\left(x_j\right)\right)}{m - n + 1}, \tag{6}$$

where there are $m$ experimental targets and $n$ variable parameters $x_i$. The standard error of the fit provides insight into the effect of parameter variation on the fit itself and is given by

$$\sigma_f = \sqrt{diag\left(\mathbf{J}\left(\mathbf{J^T W J}\right)^{-1}\mathbf{J^T}\right)}. \tag{7}$$

This provides error bars on the reconstructed parameters. The asymptotic standard prediction error provides an estimate of the total fit to experimental data

$$\sigma_{f(\beta)} = \sqrt{w_i^2 + diag\left(\mathbf{J}\left(\mathbf{J^T W J}\right)^{-1}\mathbf{J^T}\right)}. \tag{8}$$

This can be utilized as a gauge of the equilibrium model (in this case VMEC) used to fit the data.

In general, we have discussed three types of error: measurement, variance, and model errors. Each experimental measurement has a unique error which is associated with the ability of a given diagnostic to resolve a measurement. Since we wish to average over some period of time we also introduce an error associated with the variance of the data during a time window. These two errors must be combine in some meaningful way to construct a weight for each measurement one wishes to match. In general, the standard deviation in a signal over a given sampling window can be calculated. Then the error associated with measurement or the standard deviation, whichever is greater, is utilized in the construction of the weight matrix. A note should be made that certain measurements do not provide unique constraints on the equilibrium. To avoid pathological local minima during the optimization these signals utilize a larger error bar. The pertinent example is that while the aforementioned method for electron temperature measurements is utilized, flux loop measurements are assumed to have a 20% error bar associated with them. This is justified as an analysis of the parameter space Jacobian indicates that magnetic measurements do not uniquely constrain the equilibrium and its associated pressure and current profiles in 3D. This should not be taken to mean that magnetics are not well fit during the reconstruction process.

*2.2. The VMEC equilibrium model*

The VMEC code solves for 3D MHD ideal equilibrium under the assumption that a continuous set of nested flux surfaces exists in the plasma. An equilibrium is calculated through a minimization of an energy functional of the form

$$W_{MHD} = \int \left( \frac{|\vec{B}|^2}{2\mu_0} + \frac{p}{\gamma - 1} \right) dV \tag{9}$$

where $\vec{B}$ is the magnetic field, $\mu_0$ is the permeability of free space, $p$ is the plasma pressure, and $\gamma$ is the adiabatic index. Minimization of this energy functional is achieved by a preconditioned steepest descent method in which variational forces are analytically calculated. The code works in inverse coordinates in which quantities are Fourier decomposed in the poloidal and toroidal direction. A multi-grid finite difference scheme is utilized in calculation of the radial derivatives.

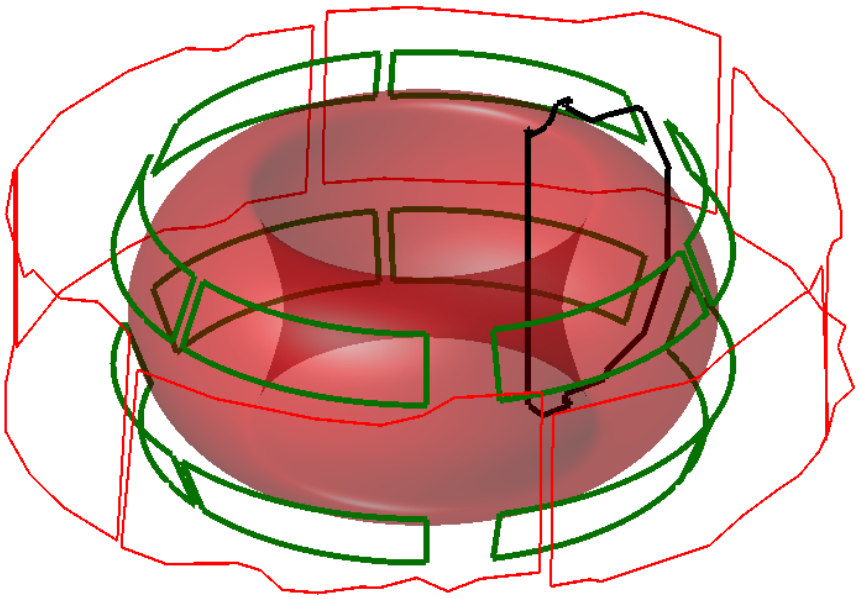

**Figure 1.** The DIII-D non-axisymmetric coil set and plasma. The RMP coils (thick green) and error field correction coils (thin red) are plotted against an axisymmetric DIII-D equilibrium. A cross section of the first-wall surface has been plotted at the DIII-D 0 degree reference datum (thick black).

The free boundary calculation in VMEC is achieved through construction of $|\vec{B}|$ on the equilibrium surface and minimizing the MHD energy functional (Eq. 9) subject to ideal variations of the boundary. The magnetic field on the equilibrium surface is constructed from the driven toroidal current inside the equilibrium boundary, vacuum field on the plasma boundary (cylindrical mesh), and a single valued potential on the surface which acts to shield out the residual normal field on the plasma boundary. In order to constrain the energy minimization the total enclosed toroidal flux of the equilibrium is prescribed. As the code minimizes the MHD energy functional,

the boundary variations are such that the resulting shape will minimize the normal component of the field (within the limits of a truncated Fourier spectrum). If a value of toroidal flux is chosen which places the boundary in a stochastic region, it is clear that the code cannot zero such a potential and must find a solution which shields out some finite normal field at its boundary. It should be noted that for a tokamak the separatrix is defined in a large part by the equilibrium itself. Thus one must consider the separatrix to lie infinitesimally outside the VMEC equilibrium (in terms of magnetic flux). The edge of the VMEC equilibrium then becomes the relevant quantity of interest. Thus the equilibrium edge is taken to be the place where plasma pressure has fallen to zero. Of course in practice there must exist a transition region where finite plasma pressure becomes comparable to neutral pressure. However, such analysis falls outside the scope of any equilibrium model. It is in this way that the effects of RMP's can be included in reconstruction.

Figure 1 depicts the 3D coils and toroidal field coils of DIII-D. The toroidal field coils, poloidal field coils, and I-coils for this shot produce a nominally 'stellarator symmetric' field for shot 142603. This symmetry implies that the equilibrium is nominally up-down symmetric in a poloidal sense and that the $\phi = 0$ plane (as defined by the coil set) is symmetry plane. The C-coils are slightly offset from the $\phi = 0$ plane requiring non-stellarator symmetric terms to model their effects (even if the equilibrium is nominally up-down symmetric). In the analysis presented here, the C-coil contribution has been neglected as have the intrinsic field errors of the device. As these two sources of non-axisymmetric field are designed to have a canceling effect on each other the neglect of both in this analysis may be justified. In general is should be noted that STELLOPT can handle non-stellarator symmetric equilibria.

The VMEC equilibrium model (and MHD equilibrium in general) requires the specification of the plasma pressure and current profiles. In experiment is it possible to measure species densities and temperatures but not the total plasma pressure. To this end a model for the plasma pressure based on the ideal gas law is utilized

$$p(s) = n_e k_B \left(T_{ion} + T_{electron}\right) + p_{fast}. \tag{10}$$

The electron density profile $n_e$, thermal ion temperature $T_{ion}$, electron temperature $T_{electron}$, and fast ion pressure $p_{fast}$ are taken to be functions of normalized toroidal flux $s$ ($k_B$ is the Boltzman constant). If a scaling factor is included in this formulation, then any mix of profiles may be utilized to constrain the profile while still matching measurements of stored energy. The DIII-D device has both Thomson and Charge Exchange allowing constraints to be placed on the electron density profile, the electron temperature profile, and the ion temperature profile. The fast ion contribution to the total pressure cannot be constrained due to difficulties in measuring the fast ions. The model equation for the total plasma pressure becomes

$$p(s) = P_{fact} n_e(s) k_B \left[T_{ion}(s) + T_{electron}(s)\right] \tag{11}$$

where $P_{fact}$ is our pressure scaling factor. In this way, variations in the species profiles translate to variations in the total pressure profile as the STELLOPT code searches for minimums in parameter space. The ability to vary $P_{fact}$ in the optimizer allows constraints on stored energy to be satisfied. This scaling factor should then contain information about the fraction of pressure accounted for by fast-ions. The assumption that the electron temperature is a function of toroidal flux can be considered accurate over most of the plasma volume. In general the ion temperature and electron density are not functions of toroidal flux. This is attributed to flow effects and the larger

ion gyro radii effects. However, the VMEC code parameterizes the plasma pressure as a flux surface function, necessitating this restriction. The result being that an equilibrium will be a flux surface averaged fit to measurements.

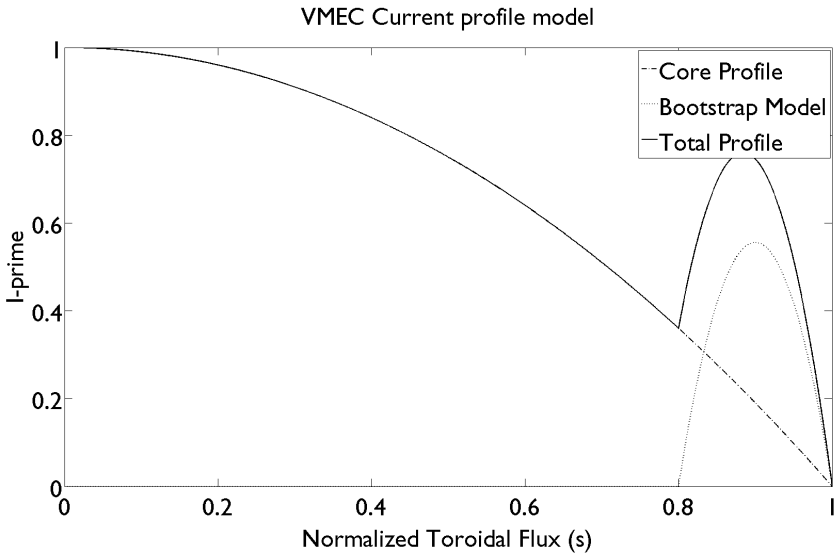


**Figure 2.** The STELLOPT net current profile model as a function of normalized toroidal flux. The core profile is modeled by a single parameter which changes the peaking of the profile. The bootstrap profile is parameterized by the height of the peak and it's location.

The net current profile in VMEC is parametrized in terms of toroidal flux as well. A variety of profile functions (in terms of the radial derivative of the flux) are provided by the code. In the reconstruction we seek to model the core current drive (containing inductive and non-inductive sources) and the edge bootstrap current. To achieve this two current profile models are summed to produce a single current profile which may be used to solve for an equilibrium (Figure 2). The core current profile is modeled as a simple power law for the current density $I'(s) = (1 - s^{\alpha})$. The edge current density is then modeled as a peaked current profile where the height and location of the peak are free parameters. The resultant profile is a linear combination of these two profile. It should be noted that internally VMEC renormalizes the profiles to the CURTOR parameter (total enclosed toroidal current). In this way the current profile itself is reduced to three free parameters: core peaking coefficient, bootstrap location, and bootstrap height. The bootstrap current is modeled as a parabola of given height and center location where it is assumed that this profile goes to zero at the edge. In this way the choice of the bootstrap location also determines the bootstrap width.

The ability to match the magnetic diagnostic response is provided by the DIAGNO code. This code was designed to calculate the magnetic diagnostic response of magnetic probes, Rogowski coils, and flux loops outside the VMEC equilibrium. It has recently been upgraded to handle various MHD equilibria [17]. This was achieved by implementation of the virtual casing principle for calculation of the magnetic field and vector potential outside the simulation domain [18]. Here the plasma currents are represented by a surface current and dipole moment density on the boundary of

the equilibrium. The DIAGNO code then performed the integrals over the diagnostics using a Simpsons rule methodology. It is then the role of STELLOPT to match the magnetic diagnostic measurements through optimization of the equilibrium input parameters.

### *2.3. The DIII-D experimental setup*

The DIII-D tokamak is a highly diagnosed Tokamak capable of accessing a wide set of plasma parameters. Magnetic diagnostics at various poloidal and toroidal locations constrain many of the plasma bulk parameters in 3D [19]. The core, edge and tangential Thomson scattering system provide a detailed set of diagnostics which constrain electron density and temperature [20]. Interferometry provides line-integrated measurements of electron density along three chords in the device for this shot [21]. The neutral beam system provides diagnostics signals for charge-exchange [22] and motional Stark effect polarimetry [23]. This constrains ion temperatures along with the toroidal current profile.

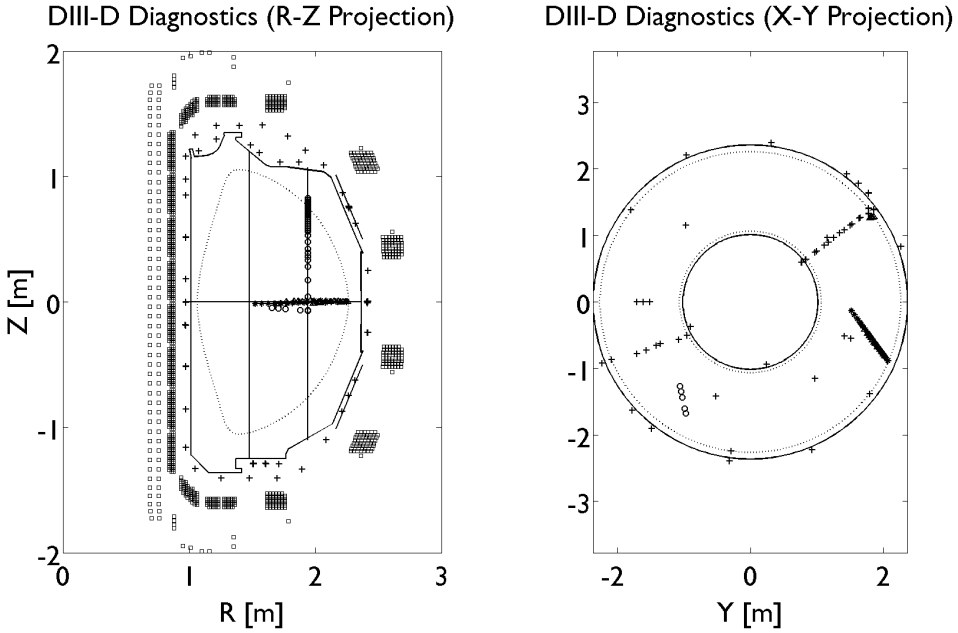


**Figure 3.** The DIII-D diagnostic set for shot 142603 mapped to the R-Z plane (left) and viewed from top down (right). The axisymmetric coils (squares), plasma limiting surface (solid line), magnetic field probes (+), Thomson data points (o), MSE data points (*), and charge exchange data points (triangles) are depicted in the plots. Solid vertical and horizontal lines in the R-Z projection indicates the line integrated density chords. Dashed line depicts a reconstructed axisymmetric boundary. Flux loops have been omitted from these plots.

Magnetic diagnostics constrain the plasma shape and bulk measurements such as stored energy and net toroidal current. For 3D systems there is no equivalent to the Grad-Shafranov equation making MHD equilibria difficult to constrain with magnetic measurements alone. Still, the interpretation of the Rogowski coil signal as net toroidal

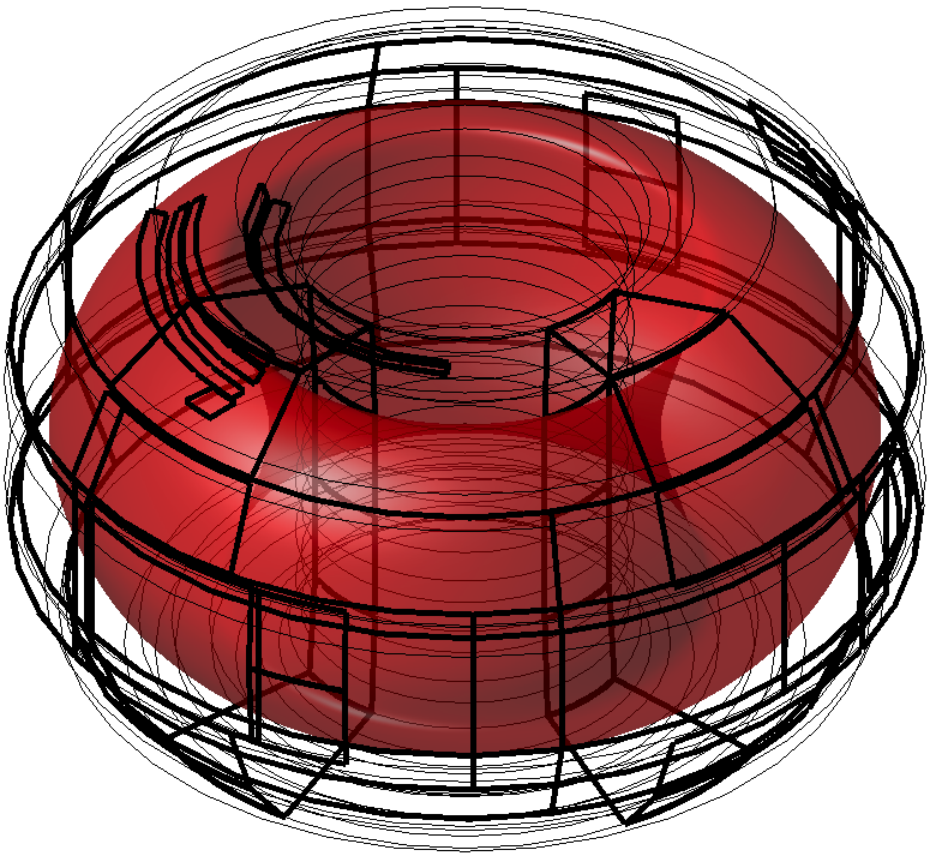

**Figure 4.** The DIII-D diagnostic flux loops with VMEC axisymmetric equilibria. The axisymmetric (thin) and saddle-loops (thick) are depicted against a VMEC axisymmetric equilibria.

current is still possible in 3D as the identity $\int \vec{B} \cdot d\vec{l} = \mu_0 I$ is still valid. Thus we may attempt to constrain the equilibrium in terms of the total toroidal current, as opposed to modeling the Rogowski coil signal directly. The flux loops and magnetic probes contain a convolution of the plasma shape, stored energy, and toroidal current (Figures 3 and 4). The utility of reconstruction, both 2D and in 3D, is the ability to deconvolve these signals and constrain the equilibrium model. Error bars for magnetic measurements are taken to be 50% the measured signal to avoid pathological local minima. This does not imply that magnetic measurements are not fit or of quality but rather that they do not uniquely constrain the 3D equilibrium.

The Thomson scattering system on DIII-D is composed of a core, lower divertor, and tangential system. Figure 3 depicts the three systems with 32 data points for the core, 8 for the divertor, and 5 for the tangent system. These measurements constrain the electron density and temperature at a set of discrete points in real space. An electron temperature cutoff of 60 $eV$ is chosen for the data, values below

this are considered to be zero signals. They are not ignored, instead they prevent STELLOPT from placing the equilibrium in regions where plasma response is most likely not important. In this way Thomson scattering can constrain the plasma edge to some extent. This is achieved by requiring the equilibrium electron temperature (and pressure) become identically zero at the boundary. It is then the goal of reconstruction to find the total enclosed toroidal flux which matches the equilibrium boundary to this location in real space. The VMEC equilibria provide a mapping from flux space to cylindrical coordinates, allowing the flux space profiles (Te, Ti, and Ne) to be compared to measured quantities in the experiment.

The CO2 interferometer system on DIII-D provides 4 chords of line-integrated electron density which help constrain the reconstruction (3 were available for this shot). This provides a convolution of profile and equilibrium shape information. To incorporate this data with the electron density measurement information from the Thomson system care must be taken to avoid inconsistencies and pathological minima. The Thomson electron density is compared in a normalized fashion. Thus amplitude information is removed from the Thomson data, thus providing feedback on profile variations alone. In this way the amplitude of the electron density profile is constrained by the line integrated measurements.

Neutral beam based diagnostics, MSE and CXRS depicted in Figure 3, provide magnetic field and ion temperature measurements at various radial and toroidal locations near the mid-plane of the device. The CXRS diagnostic provides ion temperature measurements from the core to the edge of the plasma. As the equilibrium model does not include rotation effects, the rotation as measured by CXRS is not utilized. The MSE system constrains the pitch angle of the field at various locations around the torus. A two camera system, viewing one beam from both sides, allows for the possibility of constraining the radial electric field. While radial electric fields provide no direct feedback on the equilibrium calculation, it can improve the fit to the pitch-angle data. Additionally, such data can be utilized in transport and beam deposition calculations. The electric scalar potential is parameterized as a function of normalized toroidal flux allowing the calculation of the radial electric field in the synthetic diagnostic MSE diagnostic. Radial electric field calculations have been implemented in the code but are not included in this analysis. The reconstruction is performed with the inclusion of the MSE signal but the radial electric field explicitly assumed to be zero.

## 3. Analysis

The STELLOPT code was utilized to reconstruct DIII-D shot 142603. This was a nominally up-down symmetric double null shot on DIII-D which achieved H-mode and attempted ELM suppression using an applied $n = 3$ RMP field. The application of such a field did not result in ELM suppression or mitigation. A window from 3250 to 3750 ms was chosen over which to average all data and perform a 3D reconstruction with STELLOPT, this allows comparison with a similar kinetic EFIT for this shot. Both 3D and 2D reconstructions were performed using STELLOPT to discern difference due to 3D effects from difference due to using a spectral code.

The 2D STELLOPT reconstruction of the equilibrium indicated a good agreement between STELLOPT and EFIT (Fig. 5). The VMEC boundary closely matched the EFIT separatrix on the mid plane and off the mid plane at the point where the Thomson chords intersected the equilibrium. Discrepancies near the X-points were

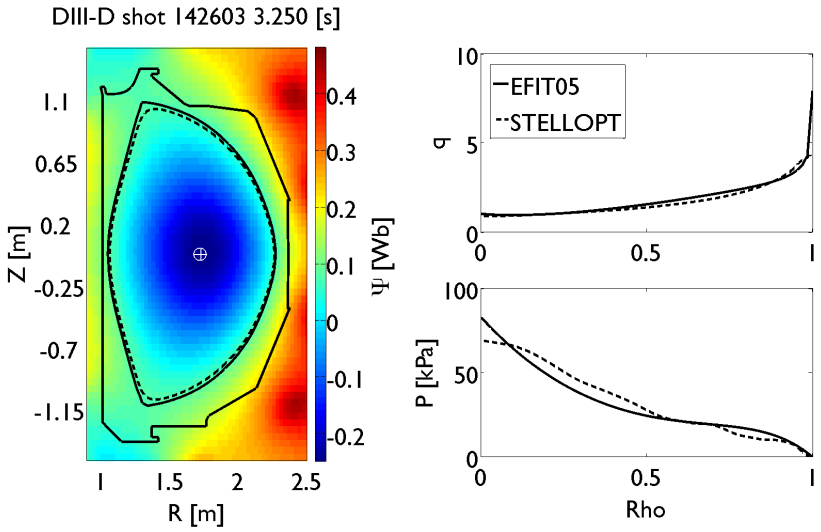


**Figure 5.** Comparison of 2D EFIT and STELLOPT reconstructions. Dotted lines indicate STELLOPT quantities while color contours indicate EFIT poloidal flux. Profiles are a function of normalized toroidal flux.

present but were attributed to the inverse nature of the VMEC equilibrium code. Similarly, discrepancies in the q profile toward the plasma edge are attributed to similar effects. Bulk parameters such as stored energy, toroidal current, and plasma beta were also in good agreement. Values for q95 and q0 were also in agreement. Such agreement suggested that the choice of equilibrium resolutions were appropriate for modeling the the DIII-D plasma (poloidal modes $0-23$ and 99 radial surfaces). Discrepancies in the pressure profile were attributed to a more detailed representation of the profiles than present in the EFIT analysis. It is likely that allowed the same representation EFIT would have recovered similar profiles to that of STELLOPT. Correlation of these flat spots with low order rationals would indicate resonant mode penetration and the possibility of small islands or shielding currents.

The reconstructed 3D STELLOPT equilibrium is depicted in Figure 6 showing in general a good agreement with the EFIT reconstruction. The edge displacement shows a general $n = 3$ feature which is attributed to the I-coils. The equilibrium toroidal mode spectrum was limited to $n = [-3, 3]$ where 48 toroidal samples of the vacuum field were utilized. The pressure profiles show similar pedestal regions while the STELLOPT reconstruction indicates a higher core pressure. Flat spots in the pressure profile also appear which were not present in the EFIT reconstruction. The safety factors seem similar with the STELLOPT q being slightly lower. At the edge q does not rise to the EFIT value but this can be associated with EFIT being able to model the equilibrium across the edge. In general the two equilibria agree well with volumes (19.38 EFIT, 18.79 $m^3$ STELLOPT), currents (1.40 EFIT, 1.40 $MA$ STELLOPT), beta (1.61 EFIT, 1.80 % STELLOPT), and q95 (3.77 EFIT, 3.95 STELLOPT). This agreement is to be expected since we expect the 3D effects to be small everywhere except perhaps near rational surfaces and that we expect the VMEC equilibrium to be located inside the separatrix as found by EFIT. It should be noted

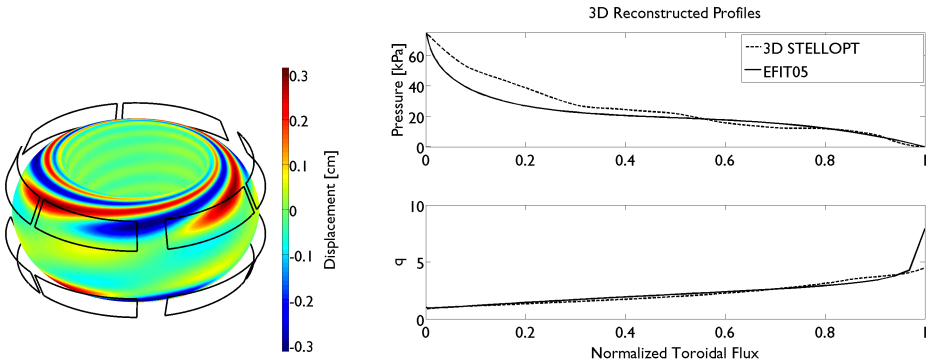


**Figure 6.** The reconstructed 3D equilibrium edge displacement (left) and reconstructed profiles (right) from STELLOPT (solid) and EFIT (dashed). A clear n=3 feature is present in the equilibrium with peak amplitudes of ±3 [mm]. The resulting pressure profile shows a slightly higher core pressure and similar pedestal feature. The profile also shows flattening in regions where EFIT had a continuous pressure gradient. The q profile shows slight differences with the largest discrepancy at the edge.

that for the q95 comparison while both values are measured at 95% toroidal flux the actual values of toroidal flux were most likely different.

The full set of magnetic probes and flux loops were utilized to constrain the plasma and the fit to data (Figure 7). The B-probes show good overall agreement with greatest discrepancy located in the diverter regions. This can be attributed to possible intrinsic error fields in the device and possibly the inverse representation of the equilibrium. Additionally these diagnostics may be sensitive to the inclusion of the C-coil fields which were not included in this calculation. Still errors were within error bars suggesting an acceptable fit to the data in nearly all probes. The axisymmetric flux loops (loops 1-44) indicate a good fit to data with the largest discrepancies located near top and bottom of the device. The non-axisymmetric flux loops (loops 45-104) also indicated a good fit to the equilibrium. Loops located near the top of the device and the two poloidal arrays indicate to good match to experiment. The larger window pane arrays located toward the outboard edge of the plasma indicate a fit in amplitude but seem to be miss some of the toroidal variation which was measured. It is thought that such residual discrepancies can be attributed to the C-coil, error-field, and the associated plasma response (which were not treated in this reconstruction).

The pressure profile was reconstructed from density and temperature measurements (Fig. 8). The electron and ion temperature profiles indicate a good fit to diagnostic measures. The VMEC edge was found to be located just outside the last non-zero values in both profiles. The electron density profile was normalized to an average of the data points within 0.05 in normalized toroidal flux. This allowed the amplitude optimization to feed back on the CO2 interferometer measurements. The radial and inner vertical chords both indicated a reconstructed line-integrated density within 1% the target value with the outer vertical chord indicating a fit within 3.8% the measured density. A pressure scaling factor of 1.16 was calculated by STELLOPT as a best match to the various diagnostic measures. The resulting beta value of 1.8% is higher than that calculated by EFIT. This could be attributed to the lack of a model for toroidal flow in VMEC. It should be noted that the resulting flat spots in

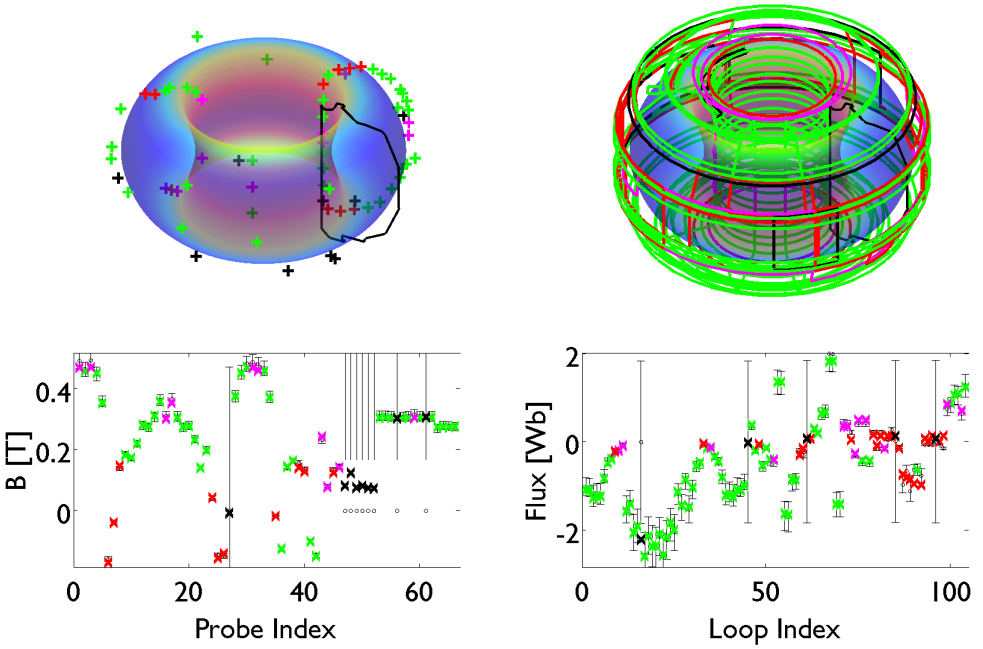


**Figure 7.** The reconstructed magnetic signals for DIII-D shot 142603. Locations of the various loops are plotted in the upper panels with the signals plotted against the measured values with STELLOPT error bars (o) below. Colors indicate quality of fit: within half an error bar (green), within error bars (magenta), greater than error bars (red), while black markers (and large error bars) indicate a signal was not utilized in the fit. The vessel cross section is plotted at the DIII-D datum. An isosurface of $|\vec{B}|$ is plotted at the VMEC boundary for reference. Non-axisymmetric flux loop signals (45-104) have been exaggerated by a factor of 20.

the pressure profile are attributed to the electron temperature profile. The flat spots were statistically significant in time and not artifacts of data averaging or noise in the dataset.

The reconstructed current profile agrees well with the motional stark effect diagnostic measure. All MSE channels agree within error bars for the reconstructed plasma parameters. Additionally the MSE signal provides a constraint on the magnetic axis location as the MSE signal covers both sides of the magnetic axis and crosses zero. The resulting reconstructed current and q-profile appear to have similar features to this of the EFIT reconstruction. The q profile approaches 1 on axis and $q95 = 3.95$. This is slightly higher than the $q95$ value as determined by EFIT, owing to difference in the edge current density. As the Lithium Beam probe was not available for this shot, the edge bootstrap current could not be constrained by local measures. The MSE signals ended at $s = 0.93$ in normalized toroidal flux, thus magnetic signals dictated the edge bootstrap current to a large extent. This is corroborated by the STELLOPT parameter space Jacobian which showed that the variation in bootstrap parameters significantly affected the magnetic probes above all other diagnostics. The MSE showed the next highest sensitivity.

Figure 10 depicts the reconstructed pressure profile plotted against the

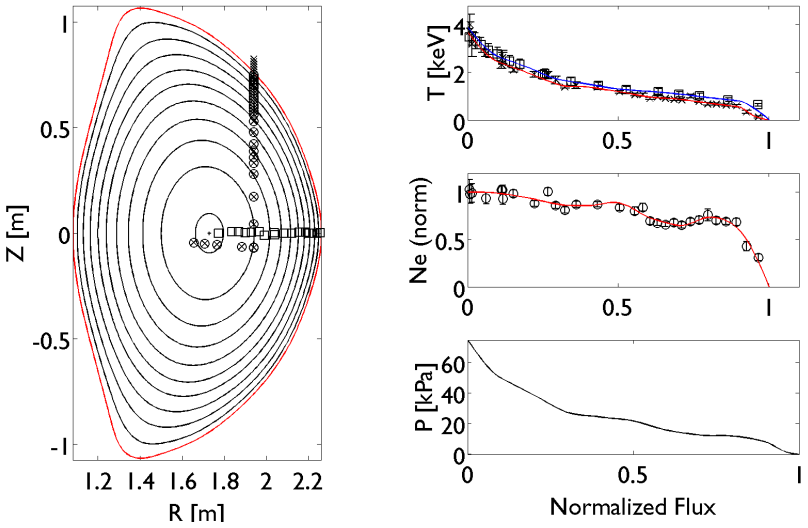


**Figure 8.** Reconstructed kinetic profiles constrained by Thomson and Charge Exchange diagnostics. Diagnostic positions are mapped to the phi=0 plane (left). Electron temperature (x, red), ion temperature (square, blue), and electron density (o, red) profiles indicate a good fit to measured values. The resulting pressure profile contains a scaling factor required to match the various diagnostics. A clear H-mode pedestal is present.

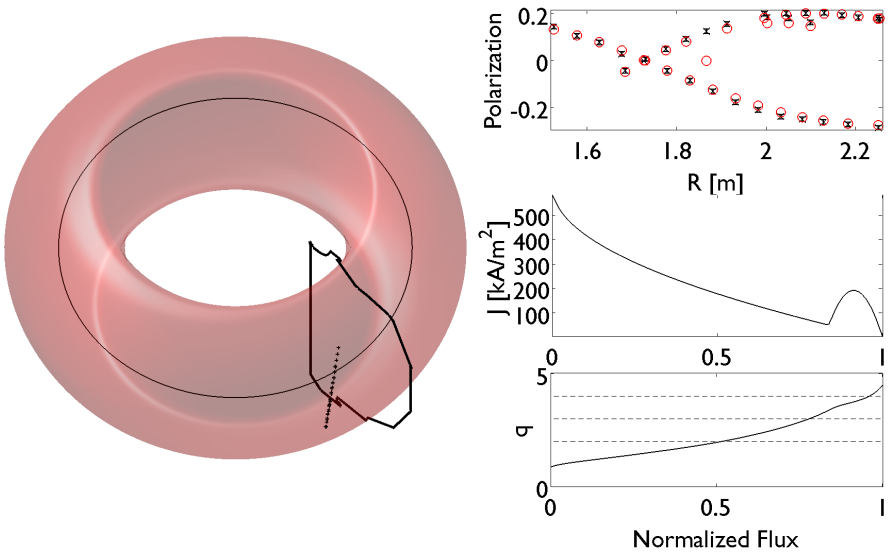


**Figure 9.** Reconstructed current profiles constrained by the motional stark effect diagnostics. Diagnostic positions are depicted with first wall outline at phi=0 (left). Measured (error bars) and reconstructed (o, red) MSE polarization are in good agreement. Current profile includes a bootstrap like bump toward the plasma edge. Reconstructed q-profile with the rational surfaces (q=2,3,4; dashed lines).

reconstructed q profile. In this plot the largest flat spot appears to be bounded by the 8/3 and 9/3 surface (centered on the 17/6) surface. As the I-coil spectrum contains both n=3 and n=6 modes, the flat spot indicates that the applied RMP has penetrated the plasma. The VMEC equilibrium lacks the ability to open islands and is only weakly sensitive to shielding effects. A more sophisticated 3D equilibrium code capable of treating islands and stochastic regions would be necessary to properly treat this region.

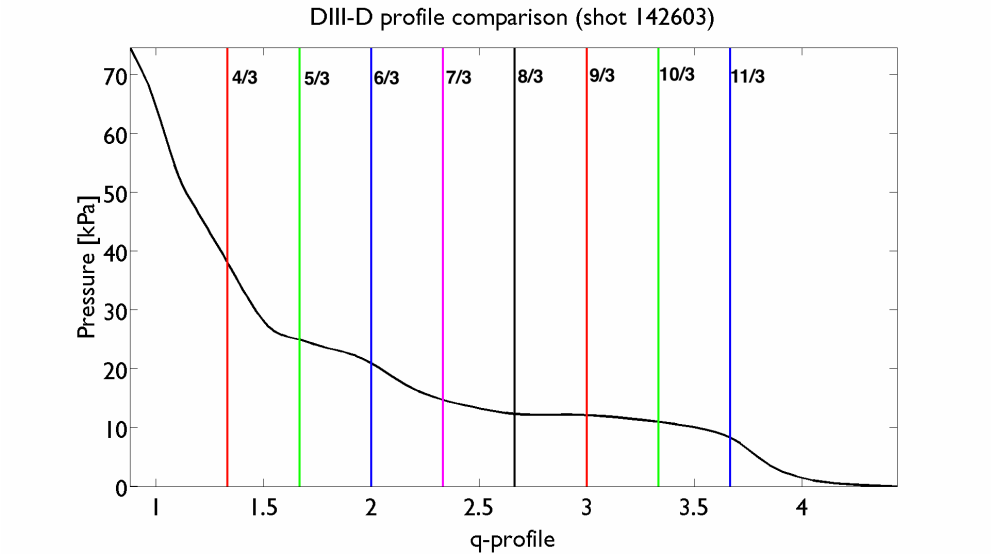


**Figure 10.** Reconstructed pressure profile plotted against the reconstructed q profile indicating flattening near low order rational surfaces. A clear flat spot appears to exist between the 8/3 and 9/3 surface which corresponds to the 17/6 surface.

A forward modeling of the bootstrap current was performed with the BOOTSJ code [24]. Here the reconstructed VMEC equilibrium and species profiles were utilized to calculate the bootstrap current. The resulting current profile agreed well with the equilibrium profile suggesting that the reconstructed bootstrap current was consistent with modeling.

## 4. Discussion

The first 3D MHD equilibrium reconstruction on DIII-D with the STELLOPT code was performed for shot 142603. This shot had applied n=3 RMPs on during the shot with no sign of ELM suppression or mitigation. The reconstructed equilibria indicated similar global features (beta, q-profile, plasma volume, toroidal current) to 2D equilibria while indicating small $\pm 3$ [mm] fluctuations in the boundary as the result of RMP application. The 3D reconstructed equilibrium profiles indicated pressure profile flattening near low-order rational surfaces and otherwise agreed well with EFIT 2D reconstructions. Current profiles allowed close matching of the MSE diagnostic although constraints on bootstrap current were limited. Modeling of the bootstrap current suggested the reconstructed bootstrap profile was adequate. A

3D reconstruction capability for the DIII-D device has now been demonstrated on a nominally up-down symmetric double null plasma.

The equilibrium model which was fit to measurements in this code allowed a three dimensional edge to be resolved. While the reconstructed equilibria indicated flattening of the pressure profile at rational surfaces, the VMEC code did not posses the ability to open islands. This can be alleviated through implementation of more advanced 3D equilibrium codes in the STELLOPT optimizer. Although the reconstruction presented here was up-down symmetric (with the shot being nominally up-down symmetric), this was only done for illustration purposes. All codes used in this work (STELLOPT, VMEC, DIAGNO) can be utilized for non-up/down symmetric equilibrium calculations. The exception being the bootstrap code (BOOTSJ). Examples of this capability are left to future works.

The set of diagnostics utilized in this work does not encompass all available diagnostics on DIII-D or more generally available to the toroidally confined magnetic fusion community. The DIAGNO code was utilized to simulate magnetic field probes and flux loops in this work, but is also capable of simulating full and segmented Rogowski coils as well. Moreover, additional synthetic diagnostics for STELLOPT are under development including Faraday rotation and X-ray imaging diagnostics. Future work will attempt to address specific situations in which 2D equilibria cannot fit edge measurements made at multiple toroidal locations.

The STELLOPT code provides researchers with the ability to fit 3D ideal MHD equilibria to diagnostic measurements in the experiment. This capability allows accurate equilibrium modeling and reduces the uncertainty associated with fitting axisymmetric equilibrium models in experiments where applied 3D field could be breaking such assumptions. Ideal perturbed modeling has already shown indications of it's breakdown near the edge when 3D fields are applied [25]. Here accurate treatment of the equilibrium edge displacement clearly requires a non-linear equilibrium model. Furthermore, the experimental interpretation of ELM suppression through applied RMPs should be evaluated with tools capable of treating the 3D plasma response in a self-consistent manner. The STELLOPT code provides such a tool.

## Acknowledgments

The author would thank D. Gates, A. Turnbull, R. Nazikian, T. Strait, and N. Ferraro for their valuable discussions on equilibrium and the DIII-D device. The author would also like to thank S. Hirshman for access to the VMEC code. A special thanks to all the diagnosticians at DIII-D for their help in sorting out the locations of all the diagnostics.

[1] T. E. Evans, R. A. Moyer, P. R. Thomas, J. G. Watkins, T. H. Osborne, J. A. Boedo, E. J. Doyle, M. E. Fenstermacher, K. H. Finken, R. J. Groebner, M. Groth, J. H. Harris, R. J. La Haye, C. J. Lasnier, S. Masuzaki, N. Ohyabu, D. G. Pretty, T. L. Rhodes, H. Reimerdes, D. L. Rudakov, M. J. Schaffer, G. Wang, and L. Zeng. Suppression of Large Edge-Localized Modes in High-Confinement DIII-D Plasmas with a Stochastic Magnetic Boundary. *Phys. Rev. Lett.*, 92(23):235003–+, 2004.

[2] K. H. Burrell, T. E. Evans, E. J. Doyle, M. E. Fenstermacher, R. J. Groebner, A. W. Leonard, R. A. Moyer, T. H. Osborne, M. J. Schaffer, P. B. Snyder, P. R. Thomas, W. P. West, J. A. Boedo, A. M. Garofalo, P. Gohil, G. L. Jackson, R. J. La Haye, C. J. Lasnier, H. Reimerdes, T. L. Rhodes, J. T. Scoville, W. M. Solomon, D. M. Thomas, G. Wang, J. G. Watkins, and L. Zeng. ELM suppression in low edge collisionality H-mode discharges using n = 3 magnetic perturbations. *Plasma Physics and Controlled Fusion*, 47:B37–B52, 2005.

[3] W. A. Cooper, J.P. Graves, O. Sauter, J. Rossel, M. Albergante, S. Coda, B.P. Duval, B. Labit,

A. Pochelon, H. Reimerdes, and the TCV team. Helical core tokamak mhd equilibrium states. *Plasma Phys. and Cont. Fusion*, 53:124005, 2011.

[4] L.L. Lao, H. St. John, R.D. Stambaugh, A.G. Kellman, and W. Pfeiffer. Reconstruction of current profile parameters and plasma shapes in tokamaks. *Nucl. Fusion*, 25:1611, 1985.

[5] LL Lao, MS Chu, AD Turnbull, MR Wade, NW Ferraro, VA Izzo, EA Lazarus, W Guo, Q Ren, R Srinivasan, et al. Plasma equilibrium response to slowly rotating 3d magnetic perturbations in diii-d rmp experiments. *Bulletin of the American Physical Society*, 56, 2011.

[6] LL Lao, NM Ferraro, RJ Buttery, TE Evans, RJ La Haye, EJ Strait, AD Turnbull, MR Wade, W Guo, MJ Lanctot, et al. Test of plasma equilibrium response against mhd models using slowly rotating 3d magnetic perturbations in\ hbox {DIII-D} rmp experiments. *Bulletin of the American Physical Society*, 57, 2012.

[7] A.M. Garofalo, R.J. LaHaye, and J.T. Scoville. Analysis and correction of the intrinsic non-axisymmetric magnetic fields in high-beta diii-d plasmas. *Nuclear Fusion*, pages 1335–1339, 2002.

[8] M.C. Zarnstorff, A. Weller, J. Geiger, E. Fredrickson, S. Hudson, J.P. Knauer, A. Reiman, A. Dinklage, G.Y. Fu, L.P. Ku, D. Monticello, A. Werner, the W7-AS Team, and the NBI-Group. Equilibrium and Stability of High-Beta Plasmas in Wendelstein 7-AS. *Fusion Sci. and Tech.*, 46, 2004.

[9] James D. Hanson, Steven P. Hirshman, Stephen F. Knowlton, Lang L. Lao, Edward A. Lazarus, and John M. Shields. V3fit: a code for three-dimensional equilibrium reconstruction. *Nuclear Fusion*, 49(7):075031, 2009.

[10] H.P. Callaghan, P.J. McCarthy, and J. Geiger. Fast equilibrium interpretation on the w7-as stellarator using function parameterization. *Nuclear Fusion*, 39(4):509, 1999.

[11] S. Sakakibara, H. Yamada, K. Watanabe, K. Yamazaki, and O. Motojima. Role of magnetic measurements for lhd equilibrium database. *J. Plasma Fusion Res.*, 1:386–389, 1998.

[12] N Pomphrey, Lang L Lao, Edward A Lazarus, M C Zarnstorff, J D Hanson, Steven P Hirshman, Stuart R Hudson, S F Knowlton, L P Ku, and D C McCune. Plasma Control for NCSX and Development of Equilibrium Reconstruction for Stellarators. In *20th IAEA Fusion Energy Conference*, Vilamoura, Portugal, November 2004. Paper IC/P6-45.

[13] D.A. Spong, S.P Hirshman, L.A. Berry, J.F. Lyon, R.H. Fowler, D.J. Strickler, M.J. Cole, B.N. Nelson, D.E. Williamson, A.S. Ware, D. Alban, R. Sànchez, G.Y. Fu, D.A. Monticello, W.H. Miner, and P.M. Valanju. Physics issues of compact drift optimized stellarators. *Nucl. Fusion*, 41:711–716, 2001.

[14] S. P. Hirshman and J. C. Whitson. Steepest-descent moment method for three-dimensional magnetohydrodynamic equilibria. *Phys. Fluids*, 26(12):3553–3568, 1983.

[15] D.E. Goldberg. *Genetic Algorithms in Search, Optimization, and Machine Learning*. Addison-Wesley, 1989.

[16] J. Pujol. The solution of nonlinear inverse problems and the levenberg-marquardt method. *Geophysics*, 72(4):W1–W16, 2007.

[17] S A Lazerson, Y. Suzuki, and S. Sakakibara. A magnetic diagnostics code for 3d toroidal systems. *Plasma Physics and Controlled Fusion*, 55(2):025014, 2013.

[18] S A Lazerson. The virtual-casing principle for 3d toroidal systems. *Plasma Physics and Controlled Fusion*, 54(12):122002, 2012.

[19] E.J. Strait. Magnetic diagnostic system of the diii-d tokamak. *Rev. of Sci. Instr.*, 77:023502, 2006.

[20] B. Bray, C. Hsieh, T.N. Carlstrom, and C.C. Makariou. Upgraded calibrations of the thomson system at diii-d. *Rev. of Sci. Instr.*, 72:1115, 2001.

[21] T N Carlstrom, D R Ahlgren, and J Crosbie. Real-time, vibration-compensated CO2 interferometer operation on the DIII-D tokamak. *Review of Scientific Instruments*, 59(7):1063, 1988.

[22] K.H. Burrell, D.H. Kaplan, P. Gohil, D.G. Nilson, R.J. Groebner, and D.M. Thomas. Improved charge coupled device detectors for the edge charge exchange spectroscopy system on the diii-d tokamak. *Rev. of Sci. Instr.*, 72:1028, 2001.

[23] D. Wróblewski, K.H. Burrell, L.L. Lao, P. Politzer, and W.P. West. Motional stark effect polarimetry for a current profile diagnostic in diii-d. *Rev. of Sci. Instr.*, 61:3552, 1990.

[24] K.C. Shaing, B.A. Carreras, N. Dominguez, V.E. Lynch, and J.S. Tolliver. Bootstrap current control in stellarators. *Phys. Fluis B1*, 1:1663–1670, 1989.

[25] A D Turnbull, N M Ferraro, V A Izzo, Edward A Lazarus, J K Park, W A Cooper, Steven P Hirshman, Lang L Lao, M J Lanctot, Samuel Lazerson, Y Q Liu, Allan H Reiman, and F Turco. Comparisons of linear and nonlinear plasma response models for non-axisymmetric perturbations. *Physics of Plasmas*, 20(5):056114, 2013.

The Princeton Plasma Physics Laboratory is operated
by Princeton University under contract
with the U.S. Department of Energy.

Information Services
Princeton Plasma Physics Laboratory
P.O. Box 451
Princeton, NJ 08543

Phone: 609-243-2245
Fax: 609-243-2751
e-mail: pppl_info@pppl.gov
Internet Address: http://www.pppl.gov